Chapter 7

# The Design of a Programmable Metal Forming Press and Its Ram Motion

Weizhong Guo and Feng Gao

Additional information is available at the end of the chapter

http://dx.doi.org/10.5772/48078l

## 1. Introduction

Metal forming is one of the oldest production processes that can be traced back to the beginning of the Industry Revolution. Today, metal forming press is still one of the most commonly used manufacturing machineries. Every day, millions of parts are produced by metal forming ranging from battery caps to automotive body panels. Therefore, even a small improvement may add to significant corporative gain.

In the early days, metal forming presses used a simple slide crank mechanism that converted the rotating motion and the energy from the unprogrammable motor to the linear motion of the ram to form the workpiece. Throughout the years, the study of the metal forming reveals the desirable press performance: smooth pressing to avoid large transient force and vibration, long dwelling time to ensure uniform metal deformation, and slow releasing to minimize workpiece spring-back.

To achieve the desirable performance, many different types of metal forming presses have been developed. In general, they can be divided into two types: mechanical presses and hydraulic presses. The former is fast (high speed presses may reach up to several thousand shots per minute) and energy efficient (the large flywheel eases the impulsive force), but lacks flexibility. The latter is flexible (their motions, including the travel and the velocity, can be programmed), but is expensive to build and to operate. This is because the hydraulic system is expensive and must be constantly pressurized during the operation with or without the metal forming work. Recently, there are programmable mechanical presses driven by servomotors. They are a newest version of the mechanical presses that is programmable and of better perfromance, e.g. low noises, excellent efficiencies and high precision for metal forming operations such as drawing, stamping, blanking, etc. Compared with traditional mechanical presses, programmable mechanical presses provide less stamping tonnage due to the capability limit of servomotors.

The programmable mechanical presses are also evolved. Since early in the nineteen nineties, several press manufacturers have been developing a couple of servo mechanical presses in series. Komatsu [1] developed servo presses whose punching forces are from 35 tons up to 200 tons. Amada [2] produced SDE series so-called digital AC servo press with a capacity of 45 tons up to 300 tons. Amino [3] developed servo press with a punching force up to 2500 tons. Chinfong [4] produces servo presses with punching forces between 80 tons and 260 tons. Heavy-duty servo mechanical presses require heavy-duty servomotors. The cost of a heavy-duty servomotor increases at exponential growth with nominal power and torque, and the capacity of the servomotor available has to be constrainted by the development of the heavy-duty servomotor technology. Currently, it is reported that the servomotors have their capacities up to 200 KW that only few manufaturers can make. Using two 200 KW servomotors, Amino developed one largest servo mechanical press with a punching force of 2500 tons in the world [3]. With the servo mechanical press growing in tonnage, it is more difficult to find such a heavy-duty servo motor at a relatively low cost, even no such heavy-duty servomotors are available. Besides the researches sponsored by the machine tool industry, some theoretical and experimental researches were performed in the universities around the world. In [5], a servomotor-driven multi-action press was designed that connected the ram to a servomotor using a bolt-screw mechanism. The desired ram motion could be generated by programming the motion of the servomotor. A double-knucle servo mechanical press with 30ton punching force was developed in [6]. In [7] a slider-crank type servo punching machine was built.

To achieve a larger tonnage, a new solution was proposed in [8-10] based on hybrid machine concept [11, 12] (see Figure 1) and developed a prototype with 25 ton (see Figure 2). This hybrid press is actuated by one common motor and one servomotor through a 2-Degree-Of-Freedom (2-DOF) linkage that the servomotor was expected to contribute only a fraction of the total energy. Currently, the hybrid press is still under development and a couple of problems need to be solved before pratical application.

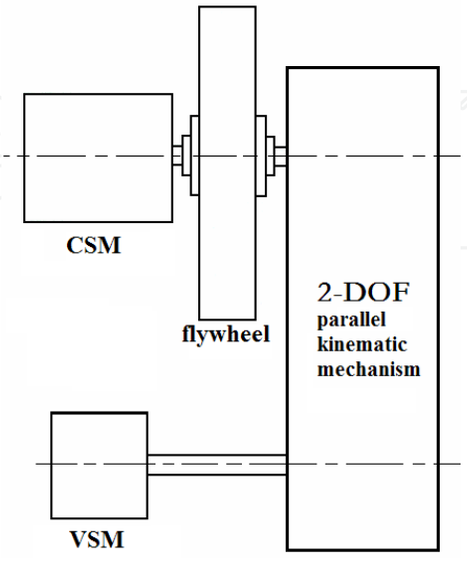


**Figure 1.** The conception of a hybrid press

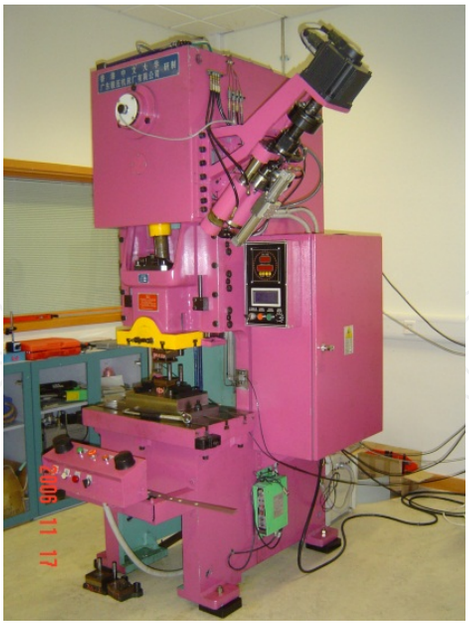

**Figure 2.** The prototype of a hybrid press

Generally, the development of a servo mechanical press mainly involves programmable actuator and control technology, punching linkage design, and ram motion design technology. For current designs, servomotors are normally used as programmable actuators. To develop heavy-duty programmable mechanical presses at relatively low cost, a new design is proposed and being developed in our laboratory to achieve higher tonnage by using more than one servomotor to drive the 1-DOF punching linkage [13]. This new scheme is called redundant actuation, or composite actuator. It provides an optional solution to heavy-duty actuation at a relatively low cost or at a higher power than single servomotor available. To combine two or more programmable actuators into a composite actuator, a 2-DOF or multi-DOF parallel mechanism is a feasible solution from a mechanical point of view (see Figure 3), similar to a yoke used between a pair of or more oxen to allow them to pull a load. In [14], several schemes of redundant actuation were proposed based on parallel mechanisms (see Figure 4). Apparently, a composite actuator should be able to act as one servomotor of large capability in terms of nominal torque, nominal power, nominal speed, and efficiency. To function as one servomotor, the mechanism to combine the programmable actuators should be of high efficiency, of high mechanical advantage and of high structural stiffness. It is obvious that a composite actuator can accommodate a slim un-synchronization of individual servomotors and even fault-tolerant of individual servomotors' disorder. Therefore, a slight difference between the motions of the two servomotors is permitted by the mechanical structure of the servo press to let the ram move freely.

In this chapter, the evolution history of the metal forming presses is outlined first and then redundant actuation scheme is discussed. The optimized design of the punching mechanism is detailed. Also, the ram motion is optimized using pseudo-NURBS expression for the stamping operation. Finally, case study is given, and a prototype with 200 t punching force is fabricated in the laboratory. The presented work provides an optional solution to the development of heavy-duty servo mechanical presses.

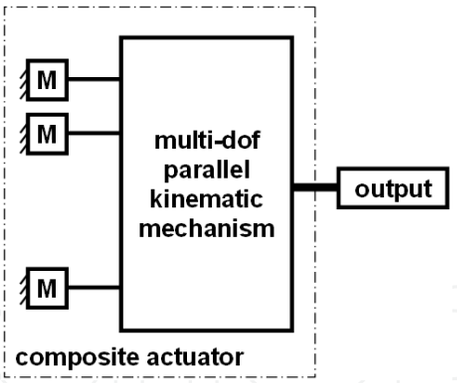


**Figure 3.** The composite actuator scheme

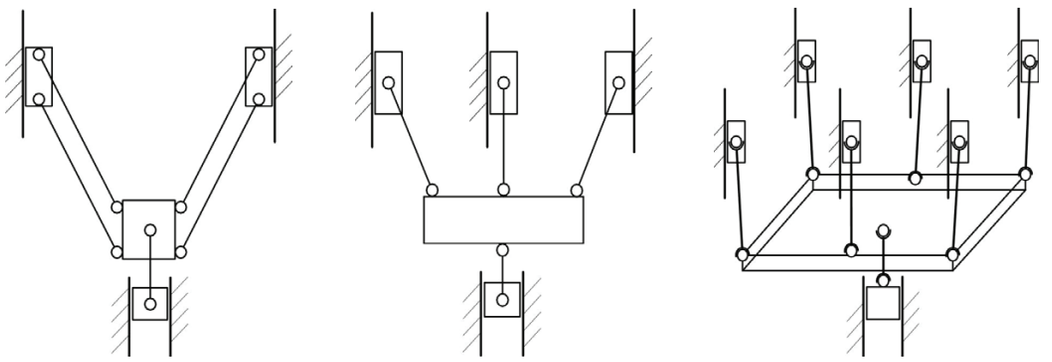

(a) 2-DOF mechanism (b) 3-DOF mechanism (c) 6-DOF mechanism

**Figure 4.** Some configurations for composite actuator design

## 2. The design of a new programmable mechanical press

In our laboratory, a servo press prototype with redundant actuation is fabricated with nominal punching force of 200 t. The design will be detailed in following sections.

### 2.1. The redundant actuation scheme

As mentioned above, two or more servomotors can be combined into a composite actuator through a 2-DOF or multi-DOF parallel mechanism. As shown in Figure 5, the presented servo mechanical press with redundant actuation uses two servomotors denoted as M to drive one input shaft which then drives a punching mechanism. These two servomotors are combined through a 2-DOF screw mechanism. To produce a high accuracy of the stamping operation, a host/slave control mode is adopted in the controller design of the servo press that the motion of one servomotor acting as host is followed by the motion of the other servomotor serving as slave. Hence, the two DOFs in the redundant actuation module avoid the bias of the ram and interference of the two servomotors while the host/slave control between the two dofs ensures high accuracy of the stamping operation. Therefore, this new scheme can provide a higher capacity with two servomotors or have a lower cost than current servo press.

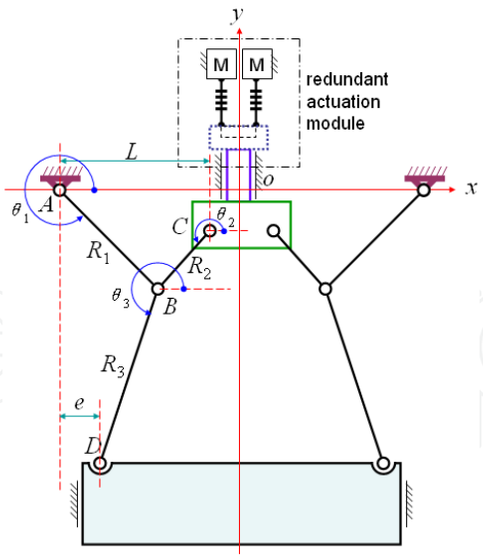


**Figure 5.** The schematics of the servo press with redundant actuation of 200 tonnage

## 2.2. The mechanism design in the redundant actuation

As discussed above, the redundant actuation scheme uses a 2-DOF screw mechanism to combine two servomotors as input of the punching mechanism. Herein, the mechanism design is one of the key problems for successful development. To design the 2-DOF mechanism, reasonable performance indices and the dimensional design should be addressed.

### *2.2.1. The performance indexing*

Generally, a machine design relates to a couple of performance indices. As to the composite actuator for the servo press, the mechanism should have a high mechanical advantage to lower the torque required from servomotors for the stamping operation. Therefore, the mechanical advantage is an important performance index for the composite actuator design. For the two servomotors, it is straightforward to use mechanical advantage reciprocals of the mechanism as performance indices derived according to theoretical mechanics as follows:

$$\eta_{ma1} = \frac{M_{in1}}{F_{out}} = \frac{L_1}{2\pi} \cdot \frac{\cos\theta_1 \sin(\phi_2 + \theta_2 - \delta)}{\cos\delta \sin(\phi_2 + \theta_2 - \phi_1 - \theta_1)} \tag{1}$$

$$\eta_{ma2} = \frac{M_{in2}}{F_{out}} = \frac{L_2}{2\pi} \cdot \frac{\cos\theta_2 \sin(\phi_1 + \theta_1 - \delta)}{\cos\delta \sin(\varphi_2 + \theta_2 - \phi_1 - \theta_1)} \tag{2}$$

$$\eta_{ma} = \frac{M_{in1} + M_{in2}}{F_{out}} = \frac{L_1 \cos\theta_1 \sin(\phi_2 + \theta_2 - \delta) + L_2 \cos\theta_2 \sin(\phi_1 + \theta_1 - \delta)}{2\pi \cos\delta \sin(\varphi_2 + \theta_2 - \phi_1 - \theta_1)} \tag{3}$$

where, $M_{in1}$, $M_{in2}$ and $F_{out}$ are two input torques and output force of the mechanism respectively. As shown in Figure 6, $L_1$ and $L_2$ are leads of the two screw rods between the servomotors and the mechanism respectively, $\phi_1$ and $\phi_2$ are angles measured from vertical

lines to two screw/slide axes respectively, $\delta$ is the angle measured from vertical line to link $l_4$, and $\theta_1$ and $\theta_2$ are angles measured from screw/slide axes to links $l_1$ and $l_2$ respectively. Obviously, $\theta_1$ and $\theta_2$ are functions of motion inputs of the servomotors.

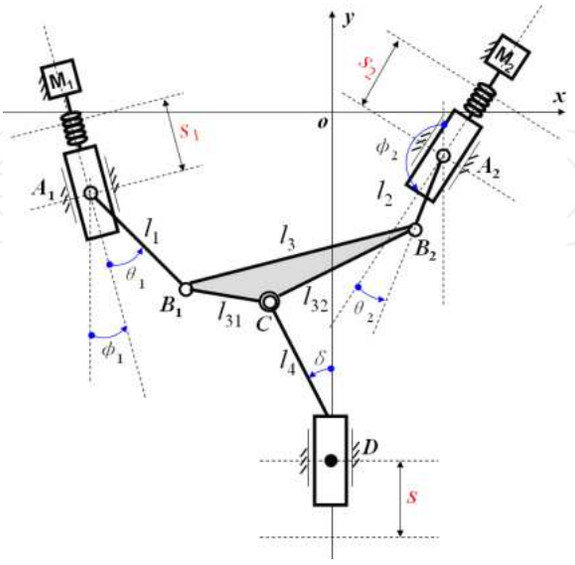


**Figure 6.** The general case for the composite actuator design

From Eq.(1), it is easy to know that the driving torques of the two servomotors are fully dependent on the mechanism configuration and the screw parameters if the inertial effects are neglected. With the change of the mechanism configuration, the mechanical advantages changes non-linearly.

### *2.2.2. Kinematic modelling*

To derive the kinematical model of the composite actuator, the Assur's Group method [15] is applied. Its basic idea is divide-and-conquer. First, the mechanism is divided into three groups: Group 1 consists of the frame and the input slide $A_1$ driven by servomotor $M_1$, Group 2 consists of the frame and the input slide $A_2$ driven by servomotor M2, and Group 3 is made of Link $A_1B_1$, Link $A_2B_2$, Link $CD$ and Link $B_1B_2C$. Next, the kinematical model for each group is derived. Finally, by combining them together, the kinematical model of the mechanism is founded.

a. Group 1: It is a Class I Assur's group. From Figure 6, it is seen that the position of the joint point $A_1$ is:

$$\begin{cases} x_1 = d_{1x} + s_1 \cos(\dfrac{3\pi}{2} + \phi_1 + \theta_1) \\ y_1 = d_{1y} + s_1 \sin(\dfrac{3\pi}{2} + \varphi_1 + \theta_1) \end{cases} \tag{4}$$

with $s_1 = s_{10} + L_1 \dfrac{\phi_1}{2\pi}$, where $s_{10}$ is the initial displacement and $\phi_1$ is the angular displacement of servomotor $M_1$. $d_{1x}$ and $d_{1y}$ are positions of the original point of slide joint $A_1$.

b. Group 2: Similar to Group 1, it is a Class I Assur's group and the position of the joint point $A_2$ is as follows:

$$\begin{cases} x_2 = d_{2x} + s_2 \cos(\frac{\pi}{2} + \phi_2 + \theta_2) \\ y_2 = d_{2y} + s_2 \sin(\frac{\pi}{2} + \phi_2 + \theta_2) \end{cases} \tag{5}$$

with $s_2 = s_{20} + L_2 \frac{\phi_2}{2\pi}$, where $s_{20}$ is the initial displacement and $\phi_2$ is the angular displacement of servomotor $M_2$. $d_{2x}$ and $d_{2y}$ are positions of the original point of slide joint $A_2$.

c. Group 3: It is an RR-RR-RP-type class-III Assur's group whose solution is numerical instead of analytical. It is modeled as an optimization question where traditional methods can be applied to find the answer. Details can be found in [15].

By single and double differentiations of the displacement formulas with respect to time respectively, the velocity and acceleration can be found as well.

### *2.2.3. Dimensional conditions and discussions*

The mechanism is a parallel mechanism having two DOFs. To make the payload distributed over the mechanical parts nearly uniformly, the mechanism should be symmetrical in configuration and dimension. Thus, we have $\phi_1 = 0^o$, $\phi_1 = 180^o$, $\delta = 0^o$, $\gamma_1 = 0^o$, $\gamma_2 = 0^o$, $l_1 = l_2$, $l_{31} = l_{32} = l_3/2$, $L_1 = L_2 = L$ for the design in Figure 6. The simplified mechanism is depicted in Figure 7.

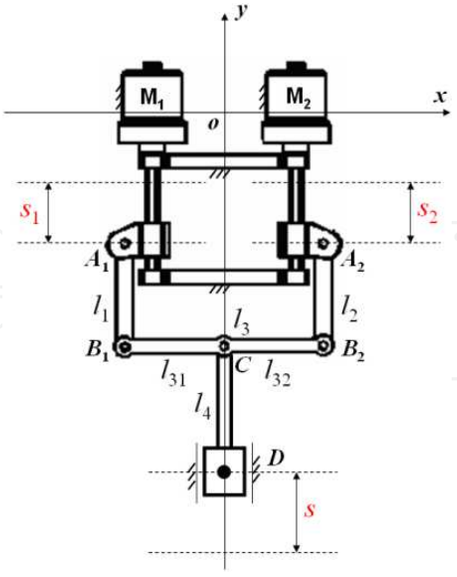


**Figure 7.** The simplified case for the composite actuator design

For the simplified mechanism, the performance indices of the mechanical advantage expressed in Eq.(1) are simplified as follows:

$$\eta_{ma1} = \frac{L}{2\pi} \cdot \frac{\cos\theta_1 \sin\theta_2}{\cos\delta \sin(\theta_2 - \theta_1)} \tag{6}$$

$$\eta_{ma2} = \frac{L}{2\pi} \cdot \frac{\cos\theta_2 \sin\theta_1}{\cos\delta \sin(\theta_1 - \theta_2)} \tag{7}$$

$$\eta_{ma} = \frac{L}{2\pi} \tag{8}$$

From Eqs.(4)-(8), it is obvious that the driving torques of the two servomotors are fully dependent on the mechanism configuration and the screw parameters if inertial effects are neglected. More importantly, although the driving torques of the two servomotors are time-variant and different, the mechanical advantage of the whole system keeps constant and is dependent on the screw lead merely. Hence, the composite actuator is able to accommodate an un-synchronization between the two servomotors without lowering the mechanical advantage. This is beneficial for the applications of compositie actuators.

## 2.3. The punching mechanism design

The punching mechanism is one of the most important parts for a mechanical press. One question for punching mechanism design is how to optimize the mechanism with better performances such as reducing torque requirement from servomotors and shortenning working cycle.

### *2.3.1. The configuration of the punching mechanism*

The servo mechanical press developed in this chapter is based on a symmetrical double-knuckle linkage as shown in Figure 5. This punching mechanism has two prismatic (P) joints and eight revolute (R) joints with five independent design parameters, including three link lengths $R_1$, $R_2$, and $R_3$, as well as two assembly distances $L$ and $e$. The upper P-joint is an active joint actuated by the redundant actuation module detailed above. The bottom P-joint is a passive joint describing the movable connection between the ram and the frame. Therefore, the bias of the ram depends on the manufacturing and assembly accuracies of the links and has no relation to the synchronization of the two servomotors.

### *2.3.2. Assembly conditions*

Half of the punching mechanism is composed of two loops. The upper loop contains Links *AB*, *BC*, the active slide *C*, and the frame. The bottom loop contains Links *AB*, *BD*, the ram slide *D*, and the frame. Considering the upper loop of the punching mechanism, the assembly condition is derived based on triangle inequality as follows:

$$\begin{aligned} R_1 + R_2 &> L \qquad \text{(a)} \\ \left|R_1 - R_2\right| &< L \qquad \text{(b)} \end{aligned} \tag{9}$$

Taking into account the on-site assembly operation, Links *AB* and *BD* are assembled firstly in gravitational line, and then Link *BC* is connected to the two links at Joint *B*. Besides, Link *BD* should be connected between Joint *B* and Joint *D* at any given configuration of the punching mechanism. Hence, the assembly offset *e* is set as 0 in this design and Links *BC* and *BD* should satisfy following relations

$$\begin{aligned} R_2 &\geq L \quad \text{(a)} \\ R_3 &> R_1 \quad \text{(b)} \end{aligned} \tag{10}$$

Besides, the knuckle formed by Links *AB* and *BD* is not expected to change folding direction during stamping operation to avoid motion fluctuation of the ram near bottom dead center (BDC). This is possible by controlling the input motion of the active P-joint.

### *2.3.3. The performance indexing*

Generally, a machine design relates to a couple of performance indices. As to the servo mechanical press, the punching mechanism should have a high mechanical advantage to lower the torque required from servomotors. Therefore, the mechanical advantage is an important performance index for the press design. For a press design, the expected tonnage of the press is known. Hence, it is straightforward to use the mechanical advantage reciprocal of the punching mechanism as a performance index that is easily derived according to theoretical mechanics as follows:

$$\eta_{ma} = \frac{F_{in}}{F_{out}} = \frac{\sin\theta_2 \sin(\theta_3 - \theta_1)}{\sin\theta_3 \sin(\theta_2 - \theta_1)} \tag{11}$$

where, $F_{\text{in}}$ and $F_{\text{out}}$ are input and output forces of the punching mechanism respectively, and $\theta_1$, $\theta_2$ as well as $\theta_3$ are angles measured from positive horizontal axis to Links *AB*, *CB* and *BD* respectively. Obviously, $\theta_1$, $\theta_2$ and $\theta_3$ are functions of input motion of the active P-joint.

Also the force distribution among the links is important for equal life cycle structure design of the parts of the servo press. Since the punching force is originated from the plastic deformation of the workpieces during stamping operation, the force distribution among the links can be measured in terms of ratio of the link force over the output force as follows:

$$\begin{aligned} \eta_1 &= \frac{\sin(\theta_2 - \theta_3)}{\sin\theta_3 \sin(\theta_2 - \theta_1)} \quad \text{(a)} \\ \eta_2 &= \frac{\sin(\theta_1 - \theta_3)}{\sin\theta_3 \sin(\theta_2 - \theta_1)} \quad \text{(b)} \\ \eta_3 &= \frac{1}{\sin\theta_3} \quad \text{(c)} \end{aligned} \tag{12}$$

where, $\eta_1$, $\eta_2$ and $\eta_3$ are related to Links *AB*, *BC* and *BD* respectively.

### *2.3.4. The dimension design with visual global optimization*

The dimension synthesis is very important for mechanism design. Current researches focus on how to build optimized design models. These models are solved by optimization methods that lead to one global/local optimized solution. Apparently, the solution depends on given conditions and/or given weighting factors for multi-goal design problems. A slim variation of the weighting factors often leads to a big change of the solution that confuses the designers. To make multi-goal optimization more straightforward, a special method was proposed by Yang, Gao and their followers that transforms the unbounded dimension space into a limited solution space [16,17], where performance atlases were displayed to show a global image of performance indices. Over these atlases, the area with global optimization is intuitive.

**a. The bounded feasible solution space**

The punching mechanism of the servo mechanical press studied in this paper is a symmetrical double- knuckle linkage with four independent design parameters, $R_1$, $R_2$, $R_3$ and $L$ as discussed above. Theoretically, the links can have their lengths up to infinity that makes the solution space an unbounded one. According to [16, 17], the link lengths can be normalized to form a limited solution space.

Let

$$\begin{aligned} r_i &= \frac{R_i}{R}, \quad i = 1,2,3 && \text{(a)} \\ l &= \frac{L}{R} && \text{(b)} \end{aligned} \tag{13}$$

where, $R = \dfrac{R_1 + R_2 + R_3 + L}{4}$, $r_i$ ($i$=1,2,3) and $l$ are normalized/non-dimensional parameters, and $R$ is an average value.

Therefore, one has

$$r_1 + r_2 + r_3 = 4 - l \tag{14}$$

Considering the assembly conditions discussed above, the normalized parameters should satisfy following relations:

$$\begin{aligned} & r_1 + r_2 > l && \text{(a)} \\ & \left| r_1 - r_2 \right| < l && \text{(b)} \\ & r_2 \geq l && \text{(c)} \\ & r_3 > r_1 && \text{(d)} \end{aligned} \tag{15}$$

Eq.(14) and inequality (15) construct the mathematic model of the bounded solution space for the servo mechanical press design. Hence, a polygonal solution slice with given $L$ can be taken

out from the solution polyhedron represented by this model as shown in Figure 8. In this figure, the feasible solution locates at the shaded triangle area surrounded by the lines of $r_2 - r_1 = l$, $r_2 = l$ and $r_3 = r_1$. Obviously, $0 < r_1 \le 2 - l$, $l \le r_2 \le (4 + l)/3$ and $(4 - 2l)/3 \le r_3 \le 4 - 2l$. The feasible solution space for the servo press design is limited by all the possible design constraints.

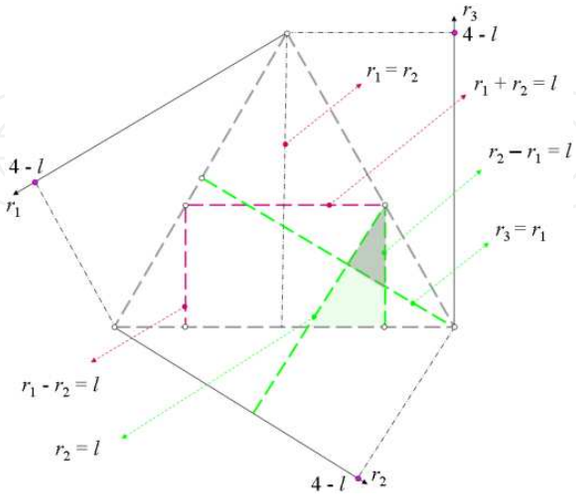


**Figure 8.** A slice of the bounded solution space for the servo press

**b. The performance atlases**

Using Eqs. (11)-(13), the performance atlases can be drawn over the bounded feasible solution space as shown in Figure 9 with respect to $r_1$, $r_2$ and $r_3$ at given $l$. Here, the maximum value of the performance indices is displayed as example. From Figure 9, it is straightforward to see the variation trend of the performance indices with respect to the deimensions. For example, it is easy to see that the force load of Link $AB$ increases and the mechanical advantage decreases while $r_2$ increases. Obviously, the performance atlases exhibit the global distribution of the perfermance indices that are helpful to the dimension synthesis leading to near global optimization.

Similar to above, any other interested performance index can be expressed as performance atlas related to link dimensions.

**c. The visual dimension design**

With the help of several performance atlases, the domain containing satisfactory solutions can be determined directly to accommodate several design goals. Then a good solution can be selected from the domain based on expertises, experiences or other rules. Also an optimized solution is able to be achieved further by optimization algorithms starting from points at the selected domain that ensures global optimization.

### *2.3.5. Case study*

To calculate the performances of different designs of servo presses, the well-known deep drawing process is introduced to calculate the performance indices. The main performance

parameters of the press are assumed as follows: (1) maximum slide stroke: 200mm; (2) travel of nominal capacity: 8mm; and (3) stroke number: 40rpm.

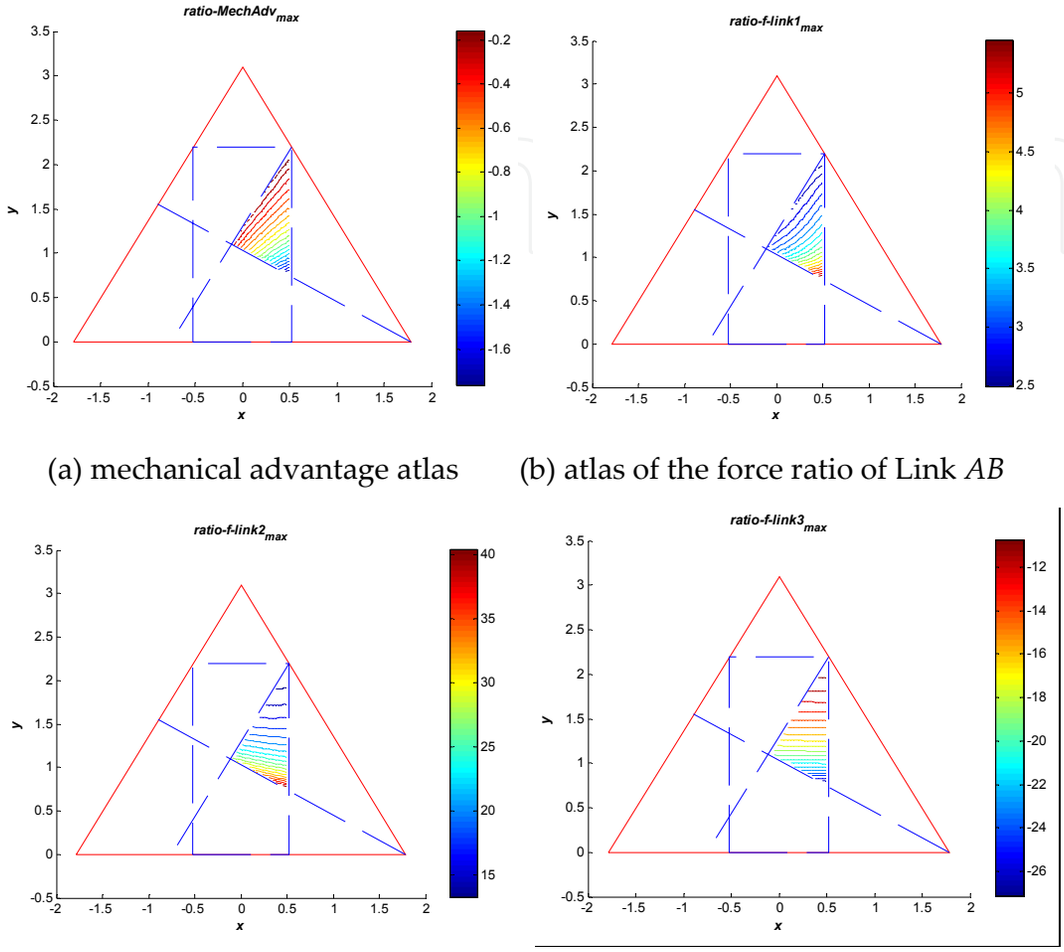


(a) mechanical advantage atlas (b) atlas of the force ratio of Link *AB*

(c) atlas of the force ratio of Link *BC* (d) atlas of the force ratio of Link *BD*

**Figure 9.** Performance atlases

| | $r_1$ | $r_2$ | $r_3$ | $L$ |
|---|---|---|---|---|
| 1 | 0.4 | 0.8 | 2.0 | 0.8 |
| 2 | 0.4 | 1.2 | 1.4 | 1.0 |
| 3 | 0.6 | 1.1 | 1.3 | 1.0 |
| 4 | 0.8 | 1.0 | 1.2 | 1.0 |
| 5 | 0.1 | 1.3 | 1.4 | 1.2 |

**Table 1.** The five design cases

Here are five cases listed in Table 1 as example. To calculate the performance indices, the average length $R$ can be set according to the maximum slide stroke 200mm. In Figure 10, the maximum mechanical advantage reciprocals within the travel of nominal capacity 8mm for the five cases are displayed over the bounded feasible solution space. The dimension points

for the middle three cases locate at one same solution slice. It can be seen that the value range grows bigger with the decreasing of $L$. From the graphs in Figure 10, the five designs can be sorted in terms of the maximum mechanical advantage reciprocals as 1, 4, 2, 3 and 5. And it is clear that to what extent the given designs approach the global optimization in terms of one performance index by observing the corresponding performance atlas. The maximum mechanical advantage reciprocals are listed in Table 2 for the five cases.

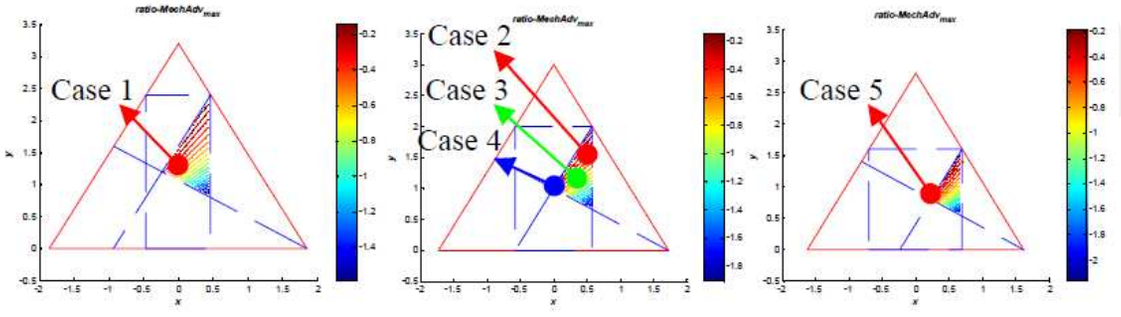


(a) the case with $L = 0.8$ (b) the cases with $L = 1.0$ (b) the case with $L = 1.2$

**Figure 10.** The designs in feasible solution space

| | Case 1 | Case 2 | Case 3 | Case 4 | Case 5 |
|---|---|---|---|---|---|
| $\eta_{ma}$ | 1.8057 | 4.0148 | 7.242 | 2.522 | 13.4863 |
| $H_1$ | 0.8057 | 3.0148 | 8.3317 | 1.522 | 12.4863 |
| $H_2$ | 2.0618 | 4.1998 | 7.8418 | 3.3132 | 13.5197 |
| $\eta_3$ | 1.0138 | 1.5874 | 2.0895 | 2.6967 | 1.3797 |

**Table 2.** The maximum performance comparisons

## 3. The design of programmable stamping operation

The most outstanding advantage of the servo press is the flexibility, i.e. the programmability of its ram motions to accommodate different stamping operations such as drawing, stamping, blanking, coining, etc. To design the stamping operation, a pseudo-NURBS method is presented to model the ram motion where the displacement and velocity demands of the stamping operation (ram motion) are transformed to weight constrains, and inequalities are formed by using weights as variables. An optimized ram motion can be generated to match the deformation of work piece material that avoids large transient force and vibration by smooth approaching and slow releasing of the ram, and improves stamping productivity via quick return of the ram.

### 3.1. The pseudo-NURBS representation of stamping operation

The ram of the press only moves along a line segment within a stroke reciprocatedly and the ram motion is changeable in terms of time. To design the ram motion, a reasonable mathematical expression should be determined firstly. As a well-known tool in computer

graphics and CAGD [18], the NURBS offers a common mathematical representation for free-form surfaces/curves and commonly used analytical shapes such as natural quadrics, torii, extruded surfaces and surfaces of revolution. It is easy and straightforward to change the shape through the manipulation of control points, weights and knots. And degree elevation, splitting, knot insertion and deletion and knot refinement offer a wide range of tools to design and analyze shape information. In this chapter, a pseudo-NURBS method is proposed to express the ram motion by introducing time parameter into the NURBS representation. A NURBS curve is a defined by the following equation:

$$c(u) = \Sigma_{i=0}^{n} \mathrm{P}_i R_{i,k}(u), \qquad R_{i,k}(u) = \frac{\omega_i N_{i,k}(u)}{\Sigma_{i=0}^{n} \omega_i N_{i,k}(u)} \tag{16}$$

where, $\mathrm{P}_i$ are vectors composed of $x$ and $y$ coordinates of the control points, $\omega_i$ are positive real weights for each control point, and point of $c(u)$ is called curve point. $R_{i,k}(u)$ are NURBS basis functions, and $N_{i,k}(u)$ are B-spline basis functions of degree $k$-1. The B-spline basis function $N_{i,k}(u)$ is expressed by de Boor-Cox [8] as follows:

$$N_{i,0}(u) = \begin{cases} 1, u_i \le u \le u_{i+1} \\ 0, otherwise \end{cases} \tag{17}$$

$$N_{i,k}(u) = \frac{u - u_i}{u_{i+k} - u_i} N_{i,k-1}(u) + \frac{u_{i+1} - u}{u_{i+k+1} - u_{i+1}} N_{i+1,k-1}(u) \tag{18}$$

where, the interval $[u_i, u_{i+1}]$ is called the $i$th knot span, and $\boldsymbol{U}=\{u_0, u_1, \ldots u_m\}$ ($m=n+k+1$) is the knot vector. A knot vector is non-periodic if the first and last knots are repeated with multiplicity $k$+1, i.e. $\boldsymbol{U}=\{u_0, \ldots, u_0, u_{k+1}, \ldots, u_{m-k-1}, u_m, \ldots u_m\}$. For most practical applications, $u_0 = 0$ and $u_m = 1$. Knots $u_{k+1}, \ldots, u_{m-k-1}$ are called interior. For planar curve, $\boldsymbol{U} = \{0, 0, 0, u_{k+1}, \ldots u_{m-k-1}, 1, 1, 1\}$.

The most significant properties of the NURBS curve are:

- Locality: A movement of the control point $P_i$ affects the curve only in the interval $[u_i, u_{i+k+1}]$.
- Affine and projective invariance: A NURBS curve is affinely and projectively invariant, i.e. transforming the curve by an affine or perspective transform is equivalent to transforming the control points.
- Differentiability: Same differentiability properties as the basis functions.

Different from the geometric shape, the time parameter $t$ should be introduced in order to express the ram motion. To apply NURBS expression for the ram motion, following issues are considered:

1. time parameter $t$: To build the relationship of the ram displacement with respect to time, the stamping time and displacement are normalized by dividing by stampling cycle and stroke respectively.
2. control points and curve points: As shown in Figure 11, the control points $P_i$ should be determined according to Eq. (16) given the curve point $Q_i$.

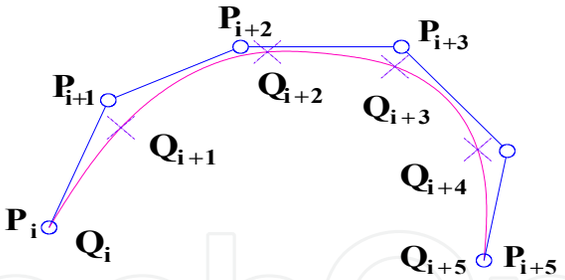


**Figure 11.** Control points and curve points

3. boundary constraints: The velocity and acceleration at the firstpoint and the endpoint should be equal to zero for the stamping cycle.
4. knot insertion. The chord method is applied as follows:

$$d = \sum_{r=1}^{n} |Q_r - Q_{r-1}| \tag{19}$$

$$t_0 = 0, \quad t_r = t_{r-1} + \frac{|Q_r - Q_{r-1}|}{d}, \quad t_n = 1 \tag{20}$$

where, $Q_r$ is curve point, $n$ is the number of the curve points, and $t_r$ is intermittent element of knot vector. The knot is expressed as

$$u_{j+p} = \frac{1}{p} \sum_{i=j}^{j+p-1} t_i \qquad j = 1, 2, \ldots, n-p \tag{21}$$

Hence, a pseudo-NURBS expression is proposed for the ram motion modeling. To assure the velocities and accelerations of the ram at the first points and endpoints zero, following constraints should be followed:

$$C^{(i)}(t_0) = D_s^{(i)}, \quad C^{(j)}(t_n) = D_e^{(j)}, \ldots\ldots i = 1, 2, \ldots, sp, j = 1, 2, \ldots, ep \tag{22}$$

where, $C^{(i)}(t_0)$ refers to $i$-th derivative at the first point, $C^{(j)}(t_n)$ means $j$-th derivative at the endpoint. Equations with the sum number of $sp$+$ep$+1 are formed from Eqs.(16) and (22) and the control points of the same number need to be determined.

$$C^{(j)}(x) = \sum_{i=0}^{n} R_{i,k}^{(j)}(x) P_i \tag{23}$$

$$R_{j,k}^{(1)}(x) = \omega_j N_{j,k}^{(1)}(x) \Big/ \sum_{i=0}^{n} \omega_i N_{i,k}(x) - \omega_i N_{j,k}(x) \sum_{i=0}^{n} \omega_i N_{i,k}^{(1)}(x) \Big/ \left[ \sum_{i=0}^{n} \omega_i N_{i,k}(x) \right]^2 \tag{24}$$

$$R_{j,k}^{(2)}(x) = \omega_j N_{j,k}^{(2)}(x) \Big/ \sum_{i=0}^{n} \omega_i N_{i,k}(x) - \left[ 2\omega_j N_{j,k}^{(1)}(x) \sum_{i=0}^{n} \omega_i N_{i,k}^{(1)}(x) + \omega_j N_{j,k}(x) \sum_{i=0}^{n} \omega_i N_{i,k}^{(2)}(x) \right]$$

$$/\left[\sum_{i=0}^{n}\omega_i N_{i,k}(x)\right]^2 + 2\omega_j N_{j,k}(x)\left[\sum_{i=0}^{n}\omega_i N_{i,k}^{(1)}(x)\right]^2 / \left[\sum_{i=0}^{n}\omega_i N_{i,k}(x)\right]^3 \tag{25}$$

$$N_{i,p}^{(j)}(x) = p\left(\frac{N_{i,p-1}^{(j-1)}(x)}{u_{i+p}-u_i} - \frac{N_{i+1,p-1}^{(j-1)}(x)}{u_{i+p-1}-u_{i+1}}\right) \tag{26}$$

Combining Eqs.(16), and (22) through (26), following equation can be got:

$$\begin{bmatrix}
1 & & & & & & & & & & & & \\
R_0^{(1)} & R_1^{(1)} & & & & & & & & & & & \\
R_0^{(2)} & R_1^{(2)} & R_2^{(2)} & & & & & & & & & & \\
 & R_1 & R_2 & R_3 & R_4 & & & & & & & & \\
 & & R_2 & R_3 & R_4 & R_5 & & & & & & & \\
 & & & R_3 & R_4 & R_5 & R_6 & & & & & & \\
 & & & & & R_5 & R_6 & R_7 & R_8 & & & & \\
 & & & & & R_5 & R_6 & R_7 & R_8 & & & & \\
 & & & & & & & R_7 & R_8 & R_9 & R_{10} & & \\
 & & & & & & & & R_8 & R_9 & R_{10} & R_{11} & \\
 & & & & & & & & & & R_{10}^{(2)} & R_{11}^{(2)} & \mathbf{R_{12}^{(2)}} \\
 & & & & & & & & & & & R_{11}^{(1)} & \mathbf{R_{12}^{(1)}} \\
 & & & & & & & & & & & & 1
\end{bmatrix}
\begin{bmatrix} P_0 \\ P_1 \\ P_2 \\ P_3 \\ P_4 \\ P_5 \\ P_6 \\ P_7 \\ P_8 \\ P_9 \\ P_{10} \\ P_{11} \\ P_{12} \end{bmatrix}
=
\begin{bmatrix} Q_0 \\ D_s^{(1)} \\ D_s^{(2)} \\ Q_1 \\ Q_2 \\ Q_3 \\ Q_4 \\ Q_5 \\ Q_6 \\ Q_7 \\ D_e^{(2)} \\ D_e^{(1)} \\ Q_8 \end{bmatrix} \tag{27}$$

By solving Eq.(27), the control points $P_0$, $P_1$…, and $P_{12}$ are determined and therefore the ram motion can be solved according to Eq.(16). Thanks to the locality of NURBS, the ram motion can be refined piecewisely through the manipulation of corresponding control points, weights and knots.

## 3.2. The influence of weights to the fluctuations of ram velocity and acceleration

To check the influence of weights to the ram motions, let [$\omega_1$] = [1, 1, 1, 1, 1, 1, 1, 1, 1, 1, 1, 1, 1], [$\omega_2$] = [1, 0.5, 0.6, 0.8, 1,0.9, 0.8, 0.4, 0.8, 1.2, 0.5, 0.8, 1], and [$\omega_3$] = [1, 1, 1, 1, 0.5, 0.6, 0.8, 0.1, 0.8, 1, 1, 1, 1]. The corresponding ram motions are dicpited in Figure 12 resepctively. It can be found that weight $\omega_i$ ($i$=8) should be adjusted that can lower the fluctuation of the ram velocity and acceleration and decrease the shock, vibration and noise during stamping operation, and decrease the peak power demand of the servomotors.

## 3.3. The influence of weights and knot vector to the fluctuations of ram velocity and acceleration

To check the influence of weights and knot vector to the ram motions, let [$\omega_1$] = [1, 1, 1, 1, 1, 1, 1, 1, 1, 1, 1, 1, 1], [$\omega_2$] = [1, 0.5, 0.6, 0.8, 1, 0.9, 0.8, 0.4, 0.8, 1.2, 0.5, 0.8, 1], [$\omega_3$] = [1, 1, 1, 1, 0.5,

0.6, 0.8, 0.05, 0.8, 1.2, 0.5, 0.8, 1], and $U_2$ = [0, 0, 0, 0, 0.0476, 0.1111, 0.254, 0.4444, 0.619, 0.7619, 0.8571, 0.92, 0.995, 1, 1, 1, 1]. The corresponding ram motions are dicpited in Figure 13 resepctively. It can be found that the peak velocity and acceleration of the return period can be lowered up to 20%-30% and the ram velocity lowered 40% when the upper die touches the workpiece by adjusting the knots corresponding to quick return period.

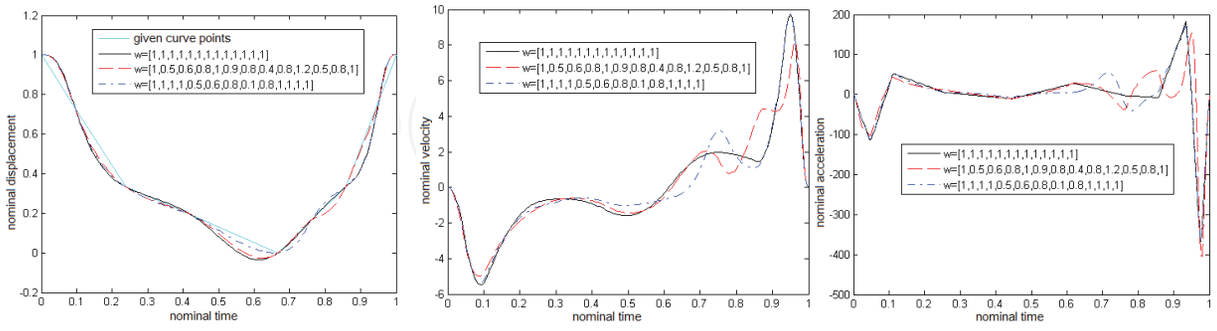


(a) displacement (b) velocity (c) acceleration

**Figure 12.** Ram motion under different weights

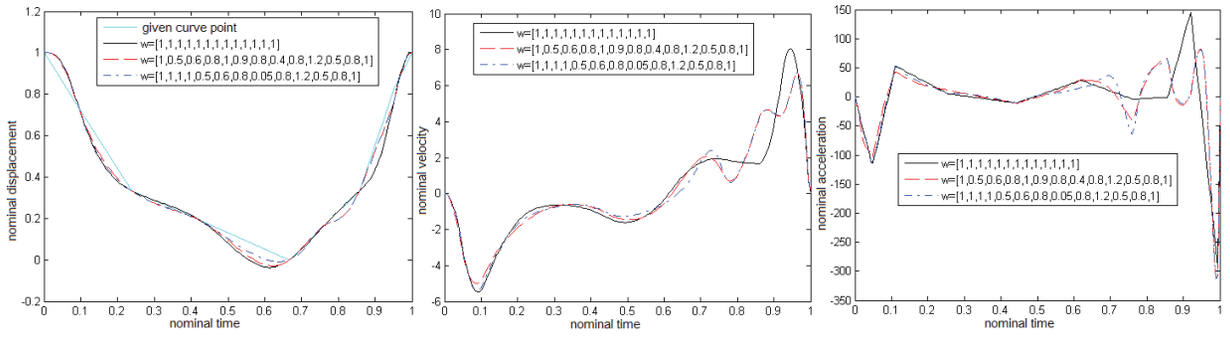


(a) displacement (b) velocity (c) acceleration

**Figure 13.** Ram motion under different weights and knot vectors

## 3.4. The self-adaption of the weights due to optimization of the ram motioin

Under the same group of demands over the displacement, velocity of the ram motion, a large number of NURBS curves can be achieved and hence the optimized one is able to select by optimization.

### *3.4.1. The self-adaption due to the ram displacement*

Due to the local support of the NURBS expression, the ram motion can be discretized into several segments to set up the constraint inequalities. The $m$ curve segments are denoted as $l_1$, $l_2$, …, and $l_m$. Supposed displacement demands over curve segement $l_j$, $s_1 \le l_j \le s_2$, i.e. $s_1 \le \frac{\sum_{i=0}^{n} d_i \omega_i N_{i,k}(u)}{\sum_{i=0}^{n} \omega_i N_{i,k}(u)} \le s_2$, where knot vector $u \in [u_{j1}, u_{j2}]$. To satisfy this in-equality demand, let

the two endpoints, maximum and minimum values over $l_j$ locate at the domain formed by $s_1$ and $s_2$, i.e.

$$s_1 \le \frac{\sum_{i=0}^{n} d_i \omega_i N_{i,k}(u_{j1})}{\sum_{i=0}^{n} \omega_i N_{i,k}(u_{j1})} \le s_2 \tag{28}$$

$$s_1 \le \frac{\sum_{i=0}^{n} d_i \omega_i N_{i,k}(u_{j2})}{\sum_{i=0}^{n} \omega_i N_{i,k}(u_{j2})} \le s_2 \tag{29}$$

$$s_1 \le \max\left( \frac{\sum_{i=0}^{n} d_i \omega_i N_{i,k}(u)}{\sum_{i=0}^{n} \omega_i N_{i,k}(u)} \right) \le s_2 \tag{30}$$

$$s_1 \le \min\left( \frac{\sum_{i=0}^{n} d_i \omega_i N_{i,k}(u)}{\sum_{i=0}^{n} \omega_i N_{i,k}(u)} \right) \le s_2 \tag{31}$$

### *3.4.2. The self-adjustment due to velocity of the ram*

Supposed velocity demand over curve section $l_j$ $v_1 \le v_{lj} \le v_2$, where $u \in [u_{j1}, u_{j2}]$. For $v_{lj} = \sum_{i=0}^{n} R'_{i,k}(u) d_i$, we have $v_1 \le \sum_{i=0}^{n} R'_{i,k}(u) d_i \le v_2$, i.e.

$$v_1 \le \sum_{i=0}^{n} \left( \frac{\dfrac{\omega_i N'_{i,k}(u)}{\sum_{j=0}^{n} \omega_j N_{j,k}(u)} - \dfrac{\omega_i N_{i,k}(u) \sum_{j=0}^{n} \omega_j N'_{j,k}(u)}{[\sum_{j=0}^{n} \omega_j N_{j,k}(u)]^2}}{} \right) d_i \le v_2 \tag{32}$$

Let $p_1 = [\sum_{j=0}^{n} \omega_j N_{j,k}(u)]^2$, $p_2 = \sum_{i=0}^{n} \left( \dfrac{\omega_i N'_{i,k}(u)}{\sum_{j=0}^{n} \omega_j N_{j,k}(u)} \right) d_i$, and $p_3 = \sum_{i=0}^{n} \left( \omega_i N_{i,k}(x) \sum_{j=0}^{n} \omega_j N'_{j,k}(x) \right) d_i$. Eq.(32) is transformed as

$$v_1 \le \frac{p_2 - p_3}{p_1} \le v_2 \tag{33}$$

To satisfy Eq.(33), make sure the values of the first point and endpoint, maximum and minimum values over $v_{lj}$ locating within the domain spaned by $v_1$ and $v_2$, i.e.

$$v_1 \le \frac{p_2(u_{j1}) - p_3(u_{j1})}{p_1(u_{j1})} \le v_2 \tag{34}$$

$$v_1 \le \frac{p_2(u_{j2}) - p_3(u_{j2})}{p_1(u_{j2})} \le v_2 \tag{35}$$

$$v_1 \le \max\left(\frac{p_2(u)-p_3(u)}{p_1(u)}\right) \le v_2 \tag{36}$$

$$v_1 \le \min\left(\frac{p_2(u)-p_3(u)}{p_1(u)}\right) \le v_2 \tag{37}$$

### *3.4.3. The solution of the optimized weights*

To lower the velocity fluctuation and ease the shock, vibration and noise to improve the workpiece's stamping quality, goal function can be defined by controlling the velocity of the ram as follows:

$$\mathrm{F}(\omega) = \min\left(\Sigma_{i=0}^{n} \mid v_i(\omega_i)\right) \tag{38}$$

where, $v_i(\omega_i) = \sum_{i=0}^{n} R'_{i,k}(u)d_i$ .

Considering some of the weights have no relation to the stamping operation, these weights are prescribed and other weights are selected to be optimized under the demands of displacement, velocity and above goal function by iterative solution.

## 3.5. Case study

### *3.5.1. The problem definition*

Take the deep drawing operation as example. The performance demands include: (1) uniform stamping operation: nearly constant stamping velocity (100-300mm/s) for drawing period, (2) quick return: high ram speed (330-500mm/s) for return period, and (3) small fluctuation of ram velocity and acceleration during drawing and releasing periods.

### *3.5.2. The optimization*

To express the relationship between the ram motion and time by NURBS, the ram displacement and time are normalized firstly as follows:

$t_0 / t$ =[0, 0.67/4, 0.99/4, 1.80/4, 2.25/4, 2.97/4, 3.37/4, 3.69/4, 1], and

$s_0 / s$ =[1, 186.78/400,106.67/400,44.44/400,0,62.22/400,177.78/400,275.56/400,1].

Correspondingly, the velocity constraints are normalized to be nominal velocity $v_0$ expressed as $v_0 = \frac{t}{s}\frac{\mathrm{d}s_0}{\mathrm{d}t_0}$ . The real ram velocity can be derived as $v = \frac{s}{t}\, v_0$ .

Because weights $\omega_i$ only affects the curve shape over the knot span $[u_i, u_{i+k+1}] \in [u_k, u_{n+1}]$, here weights $\omega_3, \omega_4, \omega_5, \omega_6$ are selected as optimized variables that relate to the drawing and releasing periods. The total weights are set as $\omega$= [0.5, 1, $\omega_3$, $\omega_4$, $\omega_5$, $\omega_6$, 0.5, 1, 0.8, 0.5, 0.8, 0.7, 0.9].

To assure the continousness of ram displacement, velocity and acceleration, NURBS of $k = 3$ is applied here. The constraints relating the punching speed are listed as:

1. drawing period: -300mm/s < $v_1(t)$ < -100mm/s, and 0.99s < t <2.25s, and
2. releasing period: 330mm/s < $v_{2(t)}$ < 500mm/s, and 2.51s < t < 2.97s.

To limit the velocity fluctuation, the goal function is defined as $F(\omega) = \min(\Sigma_{i=0}^{n} | v_i |)$.

Hence, we can get the optimized weights $\omega_3$ =0.5, $\omega_4$ =0.7, $\omega_5$ =0.8, and $\omega_6$ =0.7.

### *3.5.3. Performance analysis*

As discussed above, the optimized weights are

$\omega_a$ = [0.5, 1, 0.5, 0.7, 0.8, 0.7, 0.5, 1, 0.8, 0.5, 0.8, 0.7, 0.9].

Here another two weights are set for comparison as:

$\omega_b$ = [0.5, 1, 0.9, 0.4, 0.5, 0.2, 0.5, 1, 0.8, 0.5, 0.8, 0.7, 0.9]

$\omega_c$ = [0.5, 1, 0.3, 0.5, 0.1, 1, 0.5, 1, 0.8, 0.5, 0.8, 0.7, 0.9]

Figure 14 displays the ram motion curves under weights $\omega_a$, $\omega_b$, and $\omega_c$ respectively. From the figures, it can be seen that the ram motion of $\omega_a$ is the nearest to the desired trajectory for drawing and releaseing period, the ram velocity curve of $\omega_a$ is more flat for drawing period, and the fluctuation of the ram acceleration of $\omega_a$ is the least that helps to decrease shock, vibration and noise. This is consistent with the comparison of goal functions. The goal function values are 20441, 20457 and 20606 under $\omega_a$, $\omega_b$ and $\omega_c$ respectively.

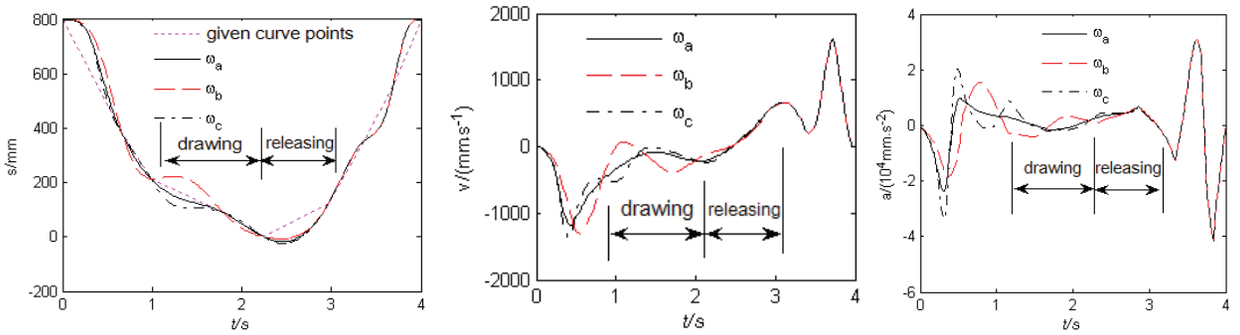


(a) displacement (b) velocity (c) acceleration

**Figure 14.** The optimized ram motion

### *3.5.4. The prototype development*

To validate the new concept, a servo press prototype with 200 ton punching force has been developed in our lab. As shown in Figure 15, the machine is more than 5 meters high and 2 meters wide. Experimental studies are being performed on this prototype including dynamic performance, dynamic control and stamping process planning.

**Figure 15.** The servo press prototype with 2-servomotor redundant actuation of 200 tonnage (photo)

## 4. Conclusion

In this chapter, a new concept of programmable metal forming press of redundant parallel actuation is presented to make it possible to develop a larger servo mechanical press using servomotors available. Based on the above discussions, following conclusions can be drawn:

1. A servo mechanical press is different from a traditional mechanical press in such a way that it involves servo actuation design with programmable motors and punching mechanism design with higher mechanical advantage.
2. The tonnage of servo mechanical presses is limited by the capacity of servomotors available to some extent. The new servo mechanical press with redundant actuation proposed in this chapter is a feasible option to develop a larger machine based on servomotors available. This redundant actuation scheme is able to accommodate an un-synchronization between the two servomotors.
3. The mechanism design for the redundant actuation should be considered carefully that maintains the performance of the redundant actuation.
4. The ram motion of the servo press can be optimized that requires a tool to express. The pseudo-NURBS representation proposed is effective to model the ram motion and form an optimization problem. Simulation shows that the optimized ram motion improves stamping operation with higher productivity and avoids large transient force and vibration by smooth approaching and slow releasing of the ram.
5. A computer programme based on the pseudo-NURBS method is developed in the laboratory embedded in the servo press that facilitates the press operation.

## Author details

Weizhong Guo and Feng Gao
*State Key Lab of Mechanical System and Vibration, Shanghai Jiao Tong University, Shanghai, China*

## Acknowledgement

The author thanks the partial financial supports under the projects from the National Natural Science Foundation of China (NSFC Grant No. 50875161), Program for New

Century Excellent Talents in University (Grant No. NCET-10-0567), the Research Fund of State Key Lab of MSV, China (Grant No.MSV-ZD-2010-02), and National Science and Technology Major Projecct, China (Grant No. 2010ZX04004-112).

## 5. References

[1] http://www.komatsusanki.co.jp
[2] http://www.amada.com
[3] http://www.amino.co.jp/index.html
[4] http://www.chinfong.com.cn/english/index.htm
[5] Shivpuri, R.S. Yossifon, A servo motor driven multi-action press for sheet metal forming, International Journal of Machinery Tool Manufacture, 1991, 31: 345-359
[6] Yossifon.S, Shivpuri.R. (1993) Design considerations for the electric servo-motor driven 30 ton double knuckle press for precision forming. International Journal of Machinery Tool Manufacture, 33(2): 209-222.
[7] Yan, H. S., Chen, W. R. (2000) On the Output Motion Characteristics of Variable Input Speed Servo-Controlled Slider-Crank Mechanisms, Mechanism and Machine Theory, 35: 541-561.
[8] R. Du, W. Z. Guo (2003) The Design of a New Metal Forming Press With Controllable Mechanism [J]. ASME Journal of Mechanical Design, 125(3): 582-592.
[9] Guo, W. Z., Du, R. (2005) A New Type of Controllable Mechanical Press-Motion Control and Experimental Validation, ASME Journal of Manufacturing Science and Engineering, 127(4): 731-742.
[10] W.Z. Guo, F. Gao, R. Du (2008) The Design and Prototype of a Servo Mechanical Press with Hybrid Inputs, Proceedings of the 8th International Conference on Frontiers of Design and Manufacturing, Sept. 23-26, 2008, Tianjin, China
[11] Tokuz, L. C. and Jones, J. R. (1991) Programmable Modulation of Motion Using Hybrid Machines, Proceedings of IMECHE, C413/071, pp. 85-91.
[12] Tokuz, L. C., 1992, Hybrid Machine Modeling and Control, Ph.D. Dissertation, Liverpool Polytechnic University.
[13] GUO Wei-zhong, GAO Feng (2009) Design of a Servo Mechanical Press with Redundant Actuation. Chinese Journal of Mechanical Engineering, 22(4): 574-579.
[14] Yongjun Bai, Feng Gao, Weizhong Guo, Yi Yue (2011) Study of the dual screw actuation for servo mechanical presses, Proceedings of 2nd IFToMM International Symposium on Robotics and Mechatronics, Shanghai, China, November 3-5, 2011
[15] Liang, C. G. and Ruan, P. S. (1986) Computer-Aided Design of Linkages, Beijing: Machine Press (in Chinese)
[16] Yang Ji-hou, Gao Feng. Solution Space and Performance Atlases of the Four-bar Mechanism [M], Beijing: China Machine Press, 1989 (in Chinese)
[17] Gao F., Zhang X.Q., Zhao Y.S., Wang H.R. (1996) A physical model of the solution space and the atlases of the reachable workspaces for 2-DOF parallel planar manipulators, Mechanism and Machine Theory, 31(2):173-184
[18] Les Piegl (1991) On NURBS: a survey, IEEE Computer Graphics & Applications, (1): 55-71.